Chapter 2

THz Measurement Systems

Leopoldo Angrisani, Giovanni Cavallo, Annalisa Liccardo, Gian Paolo Papari and Antonello Andreone

Additional information is available at the end of the chapter

http://dx.doi.org/10.5772/63734

Abstract

The terahertz (THz) frequency region is often defined as the last unexplored area of the electromagnetic spectrum. Over the past few years, the full access has been the objective of intense research efforts. Progress in this area has played an important role in opening up the possibility of using THz electromagnetic radiation (T-waves) in science and in real-world applications. T-waves are not perceptible by the human eye, are not ionizing, and have the ability to cross many non-conducting materials such as paper, fabrics, wood, plastic, and organic tissues. Moreover, the use of THz radiation allows non-destructive analysis of the materials under investigation both by study of their "fingerprint" via spectroscopic measurements and by high-resolution spatial imaging operations, exploiting the see-through capability of T-waves. Such technology can be applied in diverse areas, spanning from biology to chemical, pharmaceutical, environmental sciences, etc. In this chapter, we will present the typical architecture of measurement systems based on the THz technology, detailing what are the parameters that define their performance, the measurement methods, and the related errors and uncertainty, and focusing at the end on the use of time-domain spectroscopy for the evaluation of different material properties in this specific frequency region.

Keywords: THz measurements, THz technology, time domain spectroscopy, imaging, metrological characterization

1. Introduction to THz technology

Terahertz (THz) spectrum refers to the frequency domain ranging approximately from 100 GHz to 10 THz, corresponding to wavelengths from 3 mm to 30 μm (T-waves). The lower limit is the

microwave region, where mobile and satellite systems operate, and the upper limit is the far infrared, widely used for optical communications. **Figure 1** shows the characteristics of the T-waves in the electromagnetic (EM) spectrum.

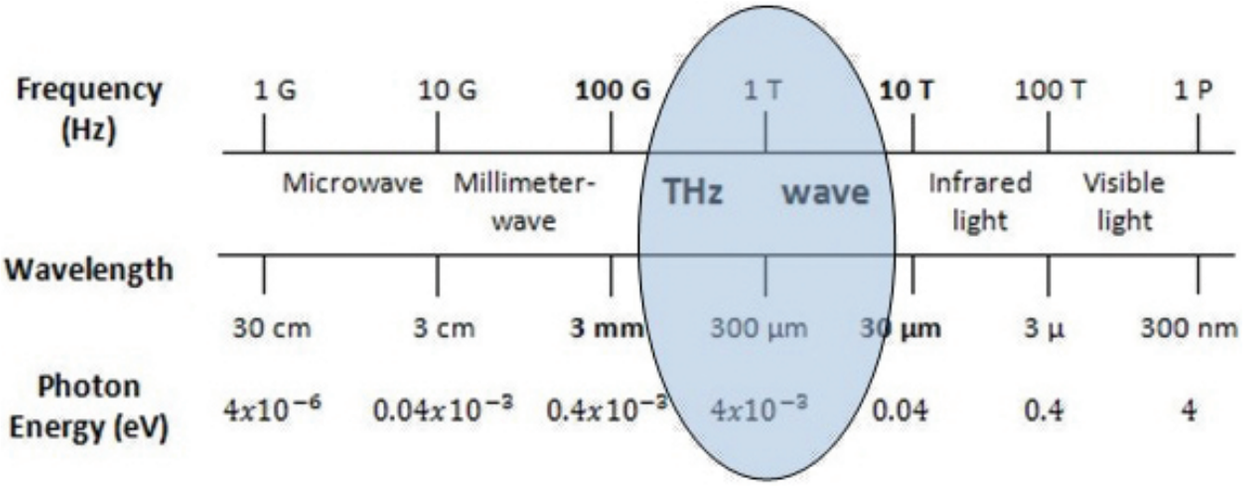

Figure 1. Position of the THz waves in the electromagnetic spectrum.

Terahertz frequency region is often defined as the last unexplored area of the EM spectrum, since it represents an area of convergence between electronics and photonics presently lacking a mature technology. Since T-waves are located between microwaves and far-infrared waves, there are two enabling technologies that can be considered for their full exploitation: electronics and photonics. Over the past 20 years, the full access and exploitation of this frequency window have been the objective of intense research efforts both in academia and in industry, in order to close the so-called THz gap. T-waves present many important properties potentially with a shattering impact both in science and in many real-world applications. First, they are not perceptible by the human eye, are not ionizing, and have the ability to cross many non-conducting common materials such as paper, fabrics, wood, plastic, and organic tissues [1, 2]. Then, in terms of energy, they give access to the rotational and vibrational modes of many molecules and macromolecules. These modes can be observed as absorption peaks in the THz spectra, providing the "fingerprint" of unknown compounds via spectroscopic measurements. Finally, the use of THz radiation allows contactless and non-destructive analysis of the materials under investigation, by spatial imaging operations [3–5] with resolution higher than micro- and millimeter waves. THz science can be applied in so many and different areas of interest, from biology to physical, chemical, pharmaceutical, and environmental research, within a broad range of industries including the medical, security, cultural heritage, manufacturing, and aerospace sectors.

The objective of this chapter is to provide readers who are not familiar with the basics of this breakthrough technology, a brief review of the typical architectures of measurement systems and the different sources and detectors that are commonly used, and looking at possible applications. Successively, they will provide details on the parameters that define the performance of a THz system, the measurement methods, and the related errors and uncertainty,

http://dx.doi.org/10.5772/63734

focusing at the end on the use of time-domain spectroscopy for the evaluation of different material properties in this specific frequency region.

2. Overview of THz sources

Since its early beginning, one of the main hurdles for the development of THz technology was a lack of solid-state signal sources, rather than detectors. Since T-waves are located between microwaves and far-infrared waves, there are two enabling technologies that can be considered for their emission: electronics and photonics.

One can roughly group THz sources into two major operational families based on the emission mode and the operating frequency: the continuous wave (CW) and the pulsed (or time domain – TD) mode [1, 6].

Most of CW systems have been developed from the electronics side, in particular the microwave field. The typical way to generate THz emission, in fact, is by scaling the frequency by using frequency multipliers. These CW systems usually operate in the lower frequency range of the THz band with maximum frequencies around 0.8 THz. Still, there are some systems able to emit at frequencies as high as 5 THz, for example backward-wave oscillators and quantum cascade lasers. Nevertheless, CW systems could be realized from the photonics side too, since down-conversion is possible by mixing two lasers that work at different frequencies [6].

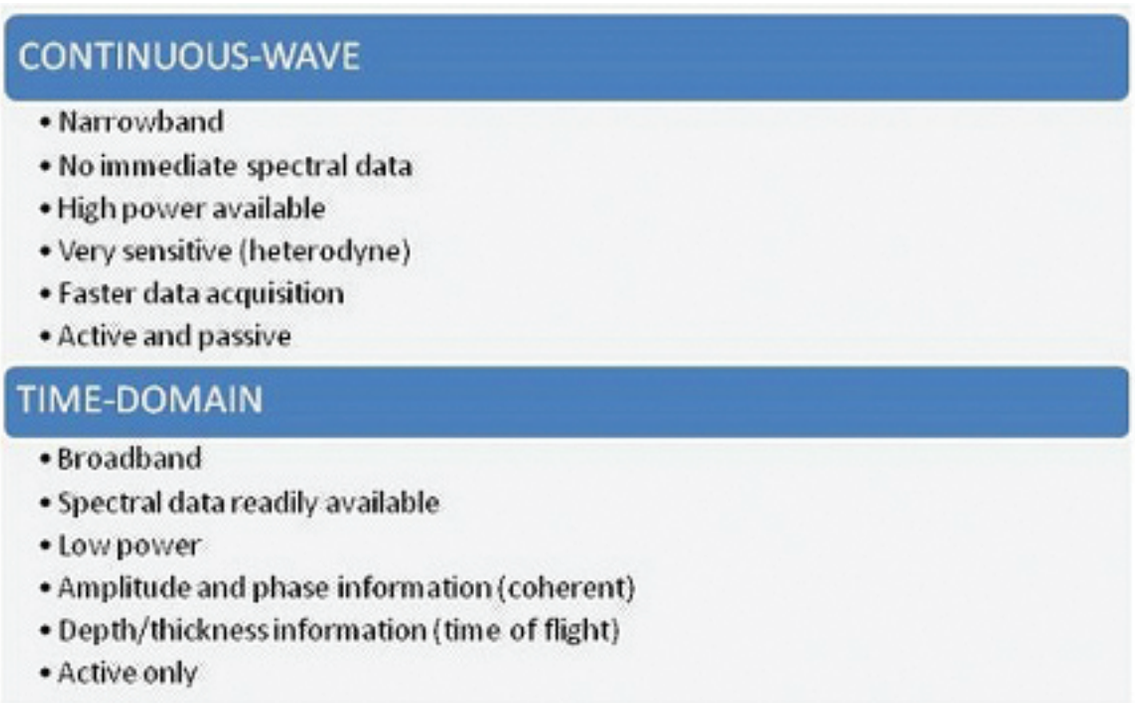

Figure 2. Characteristics of the two major operational families for the THz sources: continuous wave and time domain.

These systems are capable to operate at a single frequency, and their emission is continuous or modulated up to GHz frequencies. Therefore, CW systems are intrinsically narrowband and have often a limited tunability with a high spectral resolution (~100 MHz) very useful for gas-phase spectroscopy. Moreover, CW systems typically provide output power higher than pulsed sources. They can be passive or active; in the first case, the system detects the radiation emitted by the sample or body, whereas in the second case, the system illuminates the sample and detects the reflected or transmitted radiation. CW systems can be used in telecommunications applications and non-destructive evaluation (NDE) applications.

In pulsed or time-domain (TD) systems, the distinctive element is an optical-to-THz signal conversion technology, based on the generation and detection of an electromagnetic transient having duration of few picoseconds by means of ultrafast pulsed lasers [6]. The short pulse is composed of many frequencies, which can be accessed with a Fourier transform of the pulse. Contrary to what happens in CW systems, pulsed systems can be only active, are broadband in nature, and do not benefit of a continuous emission, so that they are ideal to study ultrafast phenomena and for general purpose spectroscopic applications.

In **Figure 2**, the major differences between CW and pulsed systems are summarized.

In the following, the most commonly used THz sources will be described, with some emphasis on those based on electro-optical conversion, since they form the base for the development of coherent systems operating in the time domain.

2.1. Backward-wave oscillator (BWO)

The backward-wave oscillator is one of the most important and successful sources based on up-conversion, allowing to extend the frequency of microwave sources to the THz range using harmonic generation. The mechanism of a BWO is very similar to a travelling wave amplifier, with the difference that it is a slow-wave structure, deliberately designed to provide feedback. In particular, a BWO seems a sophisticated high vacuum diode, where the cathode is heated by a low voltage heater and emits electrons accelerated by a high-voltage field travelling toward the anode. The electrons are collimated by a uniform external magnetic field and pass over the slow-wave structure like a comb. This mechanism produces the required quantity for the transfer of the kinetic energy of the electrons to an electromagnetic wave that builds up from noise fluctuations. The most important advantage of BWOs is their tunability; in fact, the tuning rate is ~10 MHz/V for low frequency devices, rising to ~100 MHz/V for devices operating at 1 THz or above. In addition, the output power of each BWO varies quite rapidly with frequency and the useful tuning range is approximately ±10% from the centre frequency [7].

2.2. Quantum cascade laser (QCL)

The quantum cascade laser belongs to the semiconductor-based THz sources. Over the years, the enormous progress in the field of nanotechnology is making QCL the most employed source in the CW family. In typical semiconductor lasers, light is generated by the recombination of electrons in the conduction band with holes in the valence band, separated by the

gap of the active material. In QCLs, the presence of coupled quantum wells (QWs) splits the conduction band by quantum confinement into a number of distinct sub-bands. In fact, the structure of a QLC is composed of semiconducting layered QWs from hundreds to thousands (like InGaAs/AlGaAs) [8]. Applied electric field, lifetimes, and tunneling probabilities of each level are fundamental to obtain population inversion between two sub-bands in a series of identical repeat units. The output radiation frequency is defined by the energy spacing (or QW thickness) of the lasing sub-bands. The active regions are connected with injector/collector structures allowing electrical transport through injection of carriers into the upper laser level and extraction of carriers from the lower laser level [9, 10].

2.3. Stimulated terahertz amplitude radiation (STAR) emitters

Stimulated terahertz amplified radiation (STAR) is compact and technologically simple all solid-state emitters based on superconducting devices. Coherent electromagnetic waves are generated at THz frequencies because of the Josephson effect between one or more superconductor–insulator–superconductor (SIS) junctions. Biased by a DC voltage V, a Josephson junction is essentially a two-level system with energy difference of 2 eV. As Cooper pairs are tunneling, EM waves are emitted from the junction. The radiation from a single junction, however, is only about 1 pW, and the frequency is below THz, limited in conventional low Tc superconductors by the small superconducting energy gap. The radiation power can be enhanced by fabricating an artificial array of Josephson junctions. Nevertheless, the crucial aspect relies on the coherent emission of EM waves, which requires synchronized oscillations of individual elements. The synchronization looks easier to achieve for the so-called intrinsic Josephson junctions (IJJs) that are densely packed inside high-quality single crystals of a high transition temperature Tc superconductor, usually $Bi_2Sr_2CaCu_2O_{8+\delta}$ (BSCCO). IJJs are formed naturally in BSCCO, where Bi-Sr-O layers between the superconducting CuO_2 layers act as a non-conducting barrier of nanoscale thickness [11]. The main feature rendering the STAR emitters so attractive is the nature of the emitted radiation, which is fairly robust, reasonably intense ($\sim \mu W$), and characterized by high spectral purity. Furthermore, the line width is so sharp that its observation is limited by the resolution of the conventional spectrometers (0.25 cm^{-1}). Then, the frequency of the THz radiation can be tuned considerably, approximately up to 10–15% of the central frequency, by varying the bias voltage applied to the N IJJ stack, even if its variable range of frequency strongly differs from sample to sample, depending on the preparation conditions [12].

2.4. Photoconductive antenna (PCA)

A photoconductive antenna is the most commonly used source in THz TDS systems. It consists of a semiconductor substrate where two metallic electrodes are deposited and separated by a gap of few microns. The substrate is typically a direct III-V semiconductor such as GaAs or low-temperature grown GaAs, sometimes doped silicon is adopted. In PCA, photocarriers are produced by the laser pulse and then accelerated by a bias field applied across the gap. In order to generate photo-induced free carriers, it is necessary that the photons of the laser pulse have an energy higher than the bandgap of the semiconductor. If the laser is focused at the gap

between the electrodes, the photo-induced carriers are accelerated by the bias field across the gap, which generates a current. The amplitude of the current is a function of time, and thus, the derivative of the current respect time generates the THz pulse, in fact, for the pulsed nature of the laser beam [13, 14]:

$$E_{THz} = \frac{Ae}{4\pi\varepsilon_0 c^2 z}\frac{\partial N(t)}{\partial t}\mu E_b \tag{1}$$

where A is the area under beam illumination, e the electron charge, ε_0 is the vacuum permittivity, c is the light velocity, z is the pulse penetration inside the semiconductor, N is the photocarrier density, μ is the carrier mobility, and E_b is the bias field. The main contribution to the photocurrent comes from the electrons since their mobility is often higher than that of holes. In **Figure 3**, the photoconducting antenna is excited by a fs laser pulse. The dipole structure is biased at a voltage V_{bias} to increase the THz signal emitted from the device.

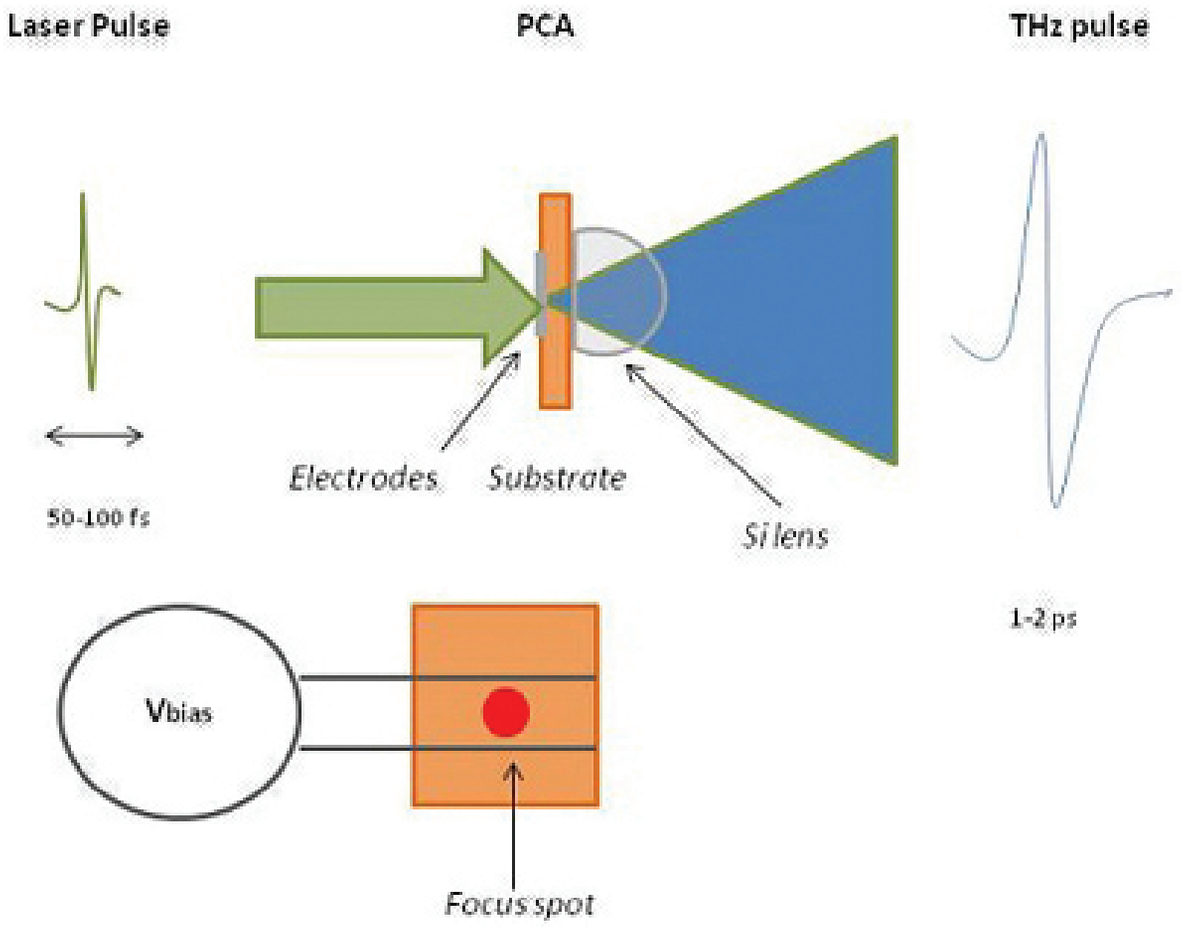

Figure 3. Sketch of the THz emission mechanism induced in a photoconductive antenna by a fs laser pulse.

Performances of PCAs can be appreciated considering some important and fundamental aspects as: semiconductor bandgap, carrier life and mobility, antenna gap and bias field. Finally, PCAs structures can be resonant or non-resonant. The first ones generate THz radiation around a central frequency, which depends on the gap distance, and the second ones have variable gap distances and provide broader frequency THz emission [13, 15].

2.5. Electro-optical conversion (EOC)

Another type of THz source is based on the electro-optical rectification. It is a nonlinear optical effect, and THz waves are generated as a result of a difference-frequency process between the frequency components contained in the femtosecond laser pulse, occurring in materials having a higher order susceptibility that is different from zero.

Mathematically, the polarization induced by the electric field associated with the optical pulse can be expressed in power series [16]:

$$\overline{P}(\bar{r},t) = \chi^{(1)}\overline{E}(\bar{r},t) + \chi^{(2)} : \overline{E}(\bar{r},t)\overline{E}(\bar{r},t) + \chi^{(3)} : \overline{E}(\bar{r},t)\overline{E}(\bar{r},t)\overline{E}(\bar{r},t) + \ldots \tag{2}$$

EO rectification comes from the second term in the previous equation. If the incident light is a plane wave, the polarization induced by the second-order susceptibility can be expressed as:

$$\overline{P}_{OR}(t) = 2\chi^{(2)} : \int_{\infty}^{0}\int_{\infty}^{0} \overline{E}(\omega+\Omega)\overline{E}'(\omega)e^{-j\Omega r}d\Omega d\omega \tag{3}$$

Here, Ω is the difference between two frequency components of the laser pulse, whereas $\chi^{(2)}$ is the second-order susceptibility, depending on the material crystalline structure. The radiated electric field due to the EO induced polarization can be expressed as follows [17, 18]:

$$\overline{E}_{THz} \propto \frac{\partial J(t)}{\partial t} = \frac{\partial^2 P(t)}{\partial t^2} = \chi^{(2)}\frac{\partial^2 E_{laser}(t)}{\partial t^2} \tag{4}$$

It is worth to emphasize that in EO rectification, no bias is necessary to realize THz generation (**Figure 4**). For a given material, the radiation efficiency and bandwidth are affected by factors such as thickness, laser pulse duration, absorption and dispersion, crystal orientation, and phase-matching conditions [19].

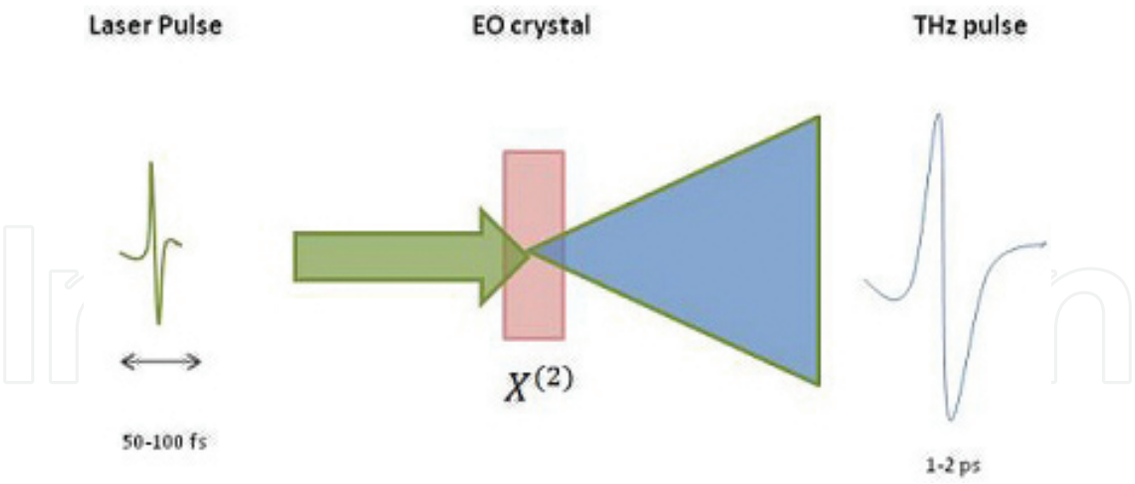

Figure 4. Sketch of the electro-optical mechanism.

2.6. Photomixing for the generation of THZ radiation

The term "photomixing" describes the generation of T-waves as a difference frequency in a nonlinear element. In the case of the THz region, it is necessary to use two IR or two visible laser photons, so that the laser frequency difference lies in this frequency range. Basically, a THz photomixer consists of two independently tunable sources (usually, solid-state diode lasers) lighting a photoconductive antenna PCA and yielding the desired difference frequency by heterodyning [20], as shown in **Figure 5**.

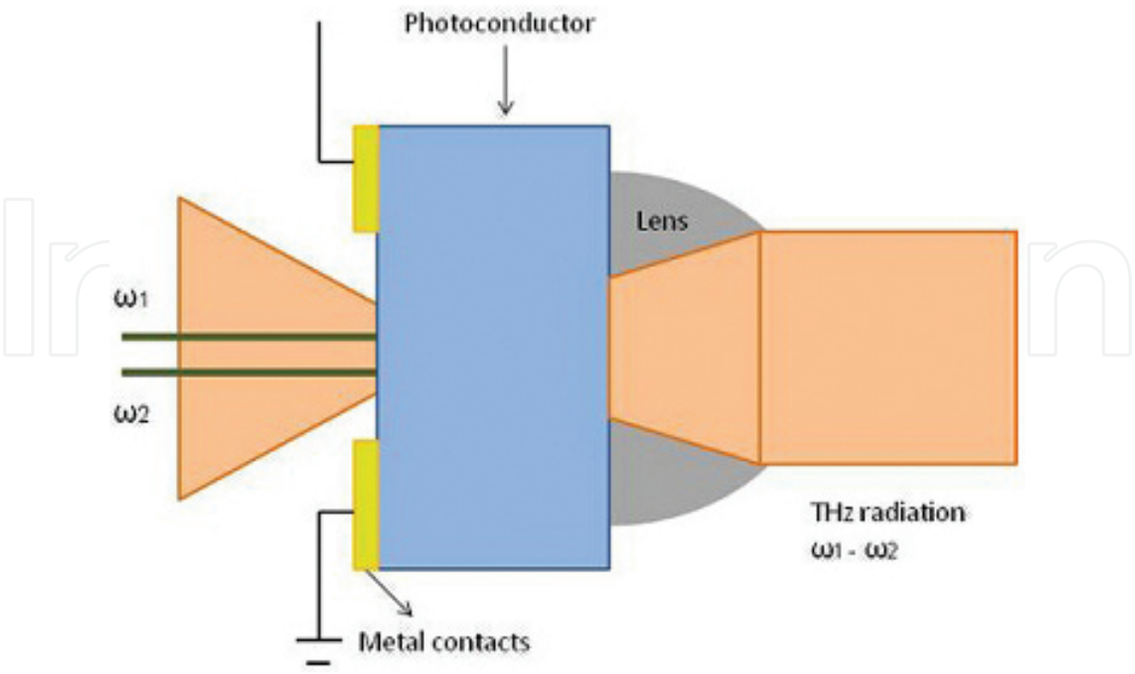

Figure 5. Operation of a THz photomixer.

The device serves as a terahertz coherent wave emitter. Changing the temperature or the operation current of the laser diodes, the value of the beat frequency can be straightforwardly regulated.

The band of the photomixer depends on the spectral width of the employed diodes; in particular, in order to enlarge the band or to move the band of the photomixer into higher frequencies, diodes with different central frequencies are necessary [21].

Table 1 summarizes the major strengths and weaknesses for the operation of the sources reported above in the THz region.

Source	Advantages	Drawbacks
BW oscillator	✓ High tunability	✗ Bulky
	✓ High output power	✗ Low frequency
QC laser	✓ High integration	✗ Small tunability
	✓ Moderate output power	✗ Low operation temperature
STAR emitter	✓ High integration	✗ Small output power
	✓ High spectral purity	✗ Low operation temperature
	✓ Moderate tunability	
Photoconductive antenna	✓ Broadband	✗ Small output power
		✗ Bulky
Electro-optical conversion	✓ Broadband	✗ Small output power
		✗ Bulky
Photomixing	✓ Moderate output power	✗ Bulky
	✓ High frequency	

Table 1. List of pros and cons for different THz sources.

3. Overview of THz detectors

In general, detectors are transducers converting an input signal into some convenient form that can be observed, recorded, and analyzed. In case of THz technology, the signal is an electromagnetic wave whose amplitude and phase both hold important information. According to the nature of EM wave, detectors can be grouped into two classes: incoherent or direct detectors that detect the amplitude only and coherent detectors that detect both amplitude and phase.

The performance of a THz detector depends on a number of parameters, some of them correlated among them. The most important are as follows: bandwidth (the spectral range over

which the detector responds), responsivity (input–output gain of the detector system), noise characteristics (characterized by the noise equivalent power, NEP, that is the signal power required to yield a signal-to-noise ratio of unity at the output of the detector in a 1 Hz bandwidth), dynamic range, response time, and sensitive area.

3.1. Thermoelectric detectors

The photon energy of a THz wave is relatively weak and comparable to the phonon energy of a crystal; for this reason, it could be detected as thermal energy. In principle, the response of such thermoelectric detectors is very slow—in the order of milliseconds—because of the thermoelectric reaction of the crystal, but it is usually ultra-broadband.

The most commonly used thermoelectric detectors are as follows: Golay cell, pyroelectric, and bolometer.

The Golay cell is a gas cell detector in which an IR-absorptive gas is encapsulated, and its thermal expansion produced by THz waves is optically detected. The pyroelectric detector is a photovoltaic detector made with a dielectric material, exhibiting temperature-sensitive surface polarization and high sensitivity to THz imaging. Typical value of NEP is 100 pW/√Hz. Finally, the bolometer is a temperature-sensitive semiconductor, such as Si or Ge, and detects the THz radiation as the change in resistivity by the heating due to absorption of THz radiation. The bolometer could operate at cryogenic temperatures, ultimately minimizing the background noise level. The typical value of NEP is $10^{-6}\mathrm{W}/\sqrt{\mathrm{Hz}}$ at 0.3 K and $1\mathrm{pW}/\sqrt{\mathrm{Hz}}$ at 300 K.

3.1.1. Golay detectors

The mechanism of a modern version of this detector, with its main features, is shown in **Figure 6**.

The main component is a sealed cell where a gas having a low thermal conductivity, usually xenon, is inserted. One side of the cell ends with a window that allows the transmission of the THz radiation in the adopted frequency interval. The other side instead is closed with a flexible mirror. The cell is completed with a thin absorbing metallic film whose impedance nearly matches that exhibited by free space. The metallic film absorbs the THz radiation thus heating the surrounding gas and causing a slight movement of the mirror. This displacement is subsequently converted into an electrical signal. In particular, a lens system is exploited to concentrate the light emitted by the source through a grid towards the mirror; then, the mirror reflects the light back to the detector through the grid. If a displacement of the mirror occurs, the reflected image of the grid is distorted, and thus, the amount of light reaching the light detector changes. For THz frequencies, the most useful window materials are high-density polyethylene (HDPE), high-resistivity Si, crystalline quartz, and diamond [22].

http://dx.doi.org/10.5772/63734

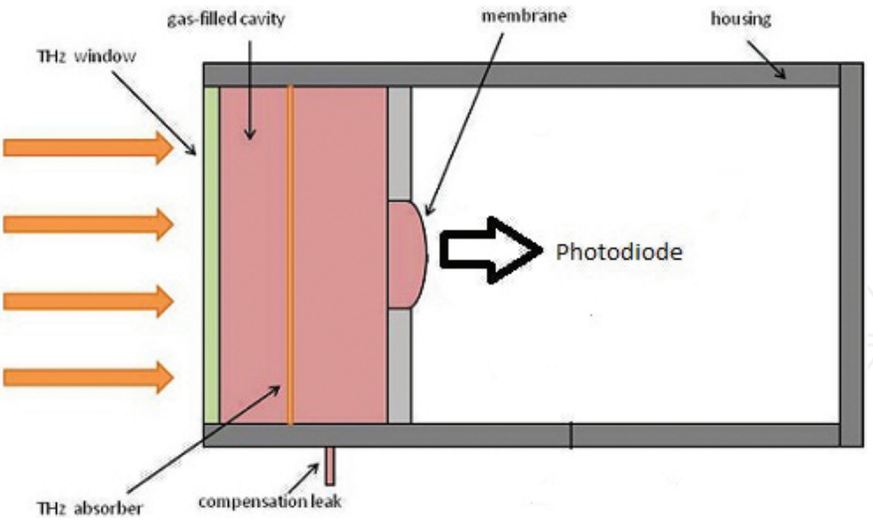

Figure 6. Structure of a Golay cell.

3.1.2. Pyroelectric detectors

A pyroelectric detector (or pyrometer) is an ac thermal sensor characterized by a frequency response spanning a large frequency range, which includes the THz region. It is based on the pyroelectric effect exhibited by a thin, permanently poled, ferroelectric crystal (i.e., $LiTaO_3$), in which the instantaneous polarization is dependent on the rate of change of the crystal temperature. Pyrometers are commercially available either as single devices or as arrays for the entire IR and THz spectral regions. Besides being very sensitive, they have many advantages, including being relatively cheap and rugged, with room temperature operation. Their most useful property is that, with appropriate design of an associated amplifier, they can exhibit response times ranging from milliseconds to less than a nanoseconds [23]. In **Figure 7**, the scheme of a pyroelectric detector and its equivalent circuital model is presented.

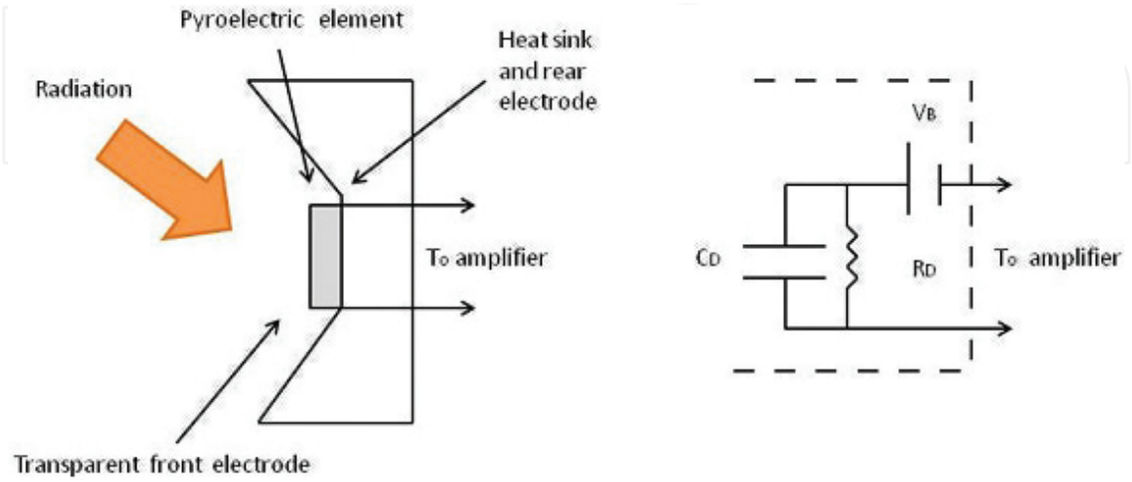

Figure 7. Pyroelectric detector and equivalent representation of electric circuit diagram.

3.1.3. Bolometer detectors

Semiconducting bolometers are among the most important of THz detectors. A design for a bolometer is shown in **Figure 8**. It consists of a small chip of doped semiconductor, Si or Ge. Typical doping concentrations are 10^{16} cm^{-3} for Ge and 10^{18} cm^{-3} for Si. The detector element is suspended in vacuum by two thin lead wires between the electrical contacts, which provide the electrical connections as well as the thermal link to the heat sink. Two aspects determine the optimum level of doping: (i) the temperature coefficient of the resistance should be large and (ii) the bolometer should have a resistance that allows for an efficient coupling to a low noise amplifier [24].

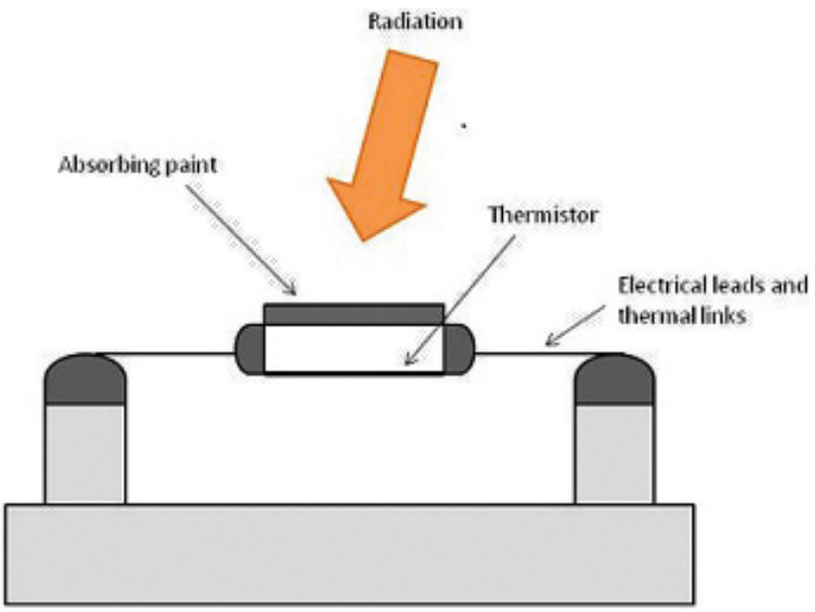

Figure 8. Simple design of a semiconducting bolometer.

A specific bolometer is the superconducting hot-spot air bolometer (SHAB), where the detector element consists of a microscopic narrow Nb or NbN strip creating a free-standing bridge structure on top of a substrate. When a voltage bias is applied to the structure, this produces the formation of a hot spot in the middle of the strip where the incoming radiation energy is dissipated, thereby switching from the superconducting to the normal state. The overall effect is a modulation of the suspended strip resistance, with a consequent modulation of the current flowing because of the voltage bias. From the recorded current, one can extract a measure of the THz radiation [25].

3.2. Photoconductive antenna

A photoconductive antenna could be considered also to detect THz waves. The structure is very similar to the structure of PCA for emission. In this case, PCA as detector measures the photocurrent, which is collected by the electrons generated by the probe beam across the antenna gap and biased by the THz electric field. When no electric field is present, the

photocarriers produced by the laser pulse move randomly and no current is observed. On the contrary, when the THz wave irradiates the gap, it generates an electric field separating electrons from holes, and therefore, a current, proportional to the amplitude of the electric field, is observed. It is important to emphasize that PCA for detection and PCA for emission are differently designed. The narrower is the gap, the lower is the electric field required for obtaining an appreciable current; therefore, PCA for detection exhibits narrower gaps (~10 μm) when compared with typical gaps of PCA for emission (> 50 μm) [14, 26, 27]. Factors affecting the performance of a PCA are similar to those for the emitter: semiconductor bandgap, carrier lifetime and mobility, and antenna gap [14].

3.3. Electro-optical sampling (EO)

Electro-optical (EO) sampling is based on the Pockels effect, in which the application of an electric field, on a material, induces or modifies the birefringence properties of it. In other words, the Pockels effect is a change in the refractive index or birefringence that depends linearly on the electric field. It is important to say that the Pockels effect can be observed only in crystals characterized by no inversion symmetry, like those belonging to the zinc-blende group such as the ZnTe [19, 27].

Using this detection method, the THz electric field is sensed by measuring the change of the birefringence properties of the crystal, caused by the field itself. These changes can be measured by analyzing the polarization properties of an optical probe beam going through the crystal. The most common setup to measure the THz waveform with EO sampling is a balanced measurement approach, as shown in **Figure 9**.

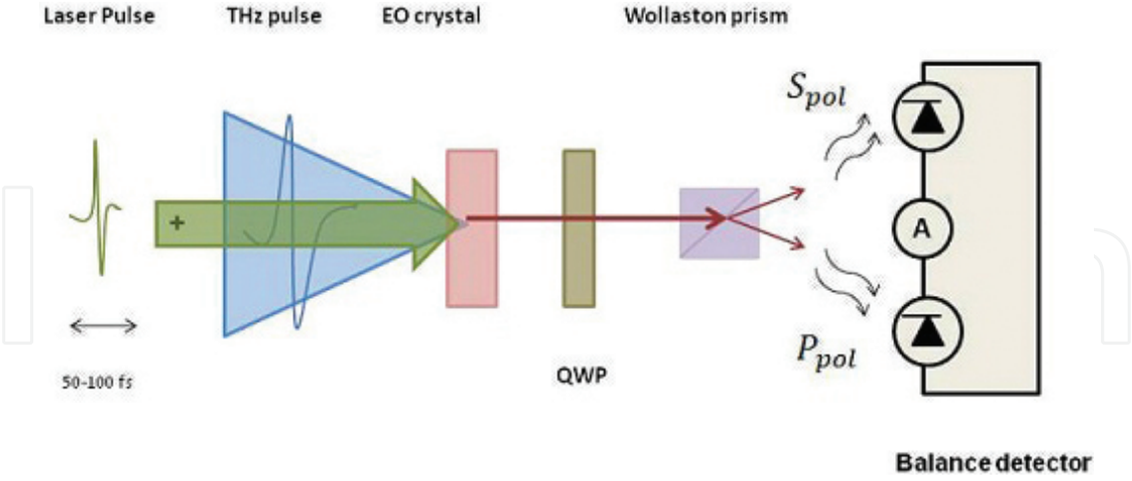

Figure 9. Sketch of the electro-optical sampling.

The operating principle is as follows. An optical probe beam characterized by linear polarization is first passed through a polarizer and then propagates within the EO crystal. A quarter-wave plate (QWP) is positioned just after the EO crystal in order to modify the probe beam ellipticity; moreover, a suitable Wollaston prism is exploited to split the elliptical polarization

into its two perpendicular components. A proper photodiode assembly mounted in differential configuration detects the diverse polarization intensity. In the absence of THz radiation impinging on the EO crystal, the probe beam ellipticity can be regulated in such a way that both polarization intensities are equal; as a consequence, the net current flowing from the differential photodiodes is equal to zero. On the contrary, when the THz wave is present, the birefringence of the EO crystal is modified by the electric field, thus changing accordingly the ellipticity of the probe beam. As a result, the balance between the two polarizations is broken and the photodiodes assembly can generated a net current whose intensity is proportional to the amplitude of the electric field associated with the impinging THz wave.

Table 2 summarizes the major strengths and weaknesses for the operation of the detectors reported above in the THz region.

Detector	Advantages	Drawbacks
Golay cell	✓ Broad spectral response	✗ Limited dynamic range
	✓ High sensitivity	✗ Slow response
	✓ Large sensing area	✗ Bulky
		✗ Fragile
		✗ Expensive
Pyrometer	✓ Broad spectral response	✗ Large NEP
	✓ High dynamic range	✗ Microphonic response
	✓ Fast response	
	✓ Compact	
	✓ Inexpensive	
Bolometer	✓ Broad spectral response	✗ Slow response
	✓ Highest sensitivity	✗ Low operation temperature
	✓ Lowest NEP	✗ Small sensing area
	✓ Compact	
Photoconductive antenna	✓ Fast response	✗ Low detection current
	✓ Moderate sensitivity	✗ Relatively expensive
Electro-optical crystal	✓ Broad spectral response	✗ Complex readout
	✓ Fast response	✗ Relatively expensive
	✓ Moderate sensitivity	

Table 2. List of pros and cons for different THz detectors.

http://dx.doi.org/10.5772/63734

4. THz systems

As already described in Section 2, the operation of THz systems can be schematically divided into continuous wave and pulsed mode.

Frequency domain (THz-CW) systems work at a fixed frequency, which depends on the type of THz emitter. As an example, in **Figure 10**, the case of a QCL source coupled to a thermal detector (a pyrometer or a bolometer) is shown. Between THz emitter and detector, there is an ellipsoidal mirror that allows to collimate the laser beam. In this configuration scheme, the reference signal produced by the source and the output signal recorded by the detector is sent to a lock-in amplifier in order to provide a coherent detection [28].

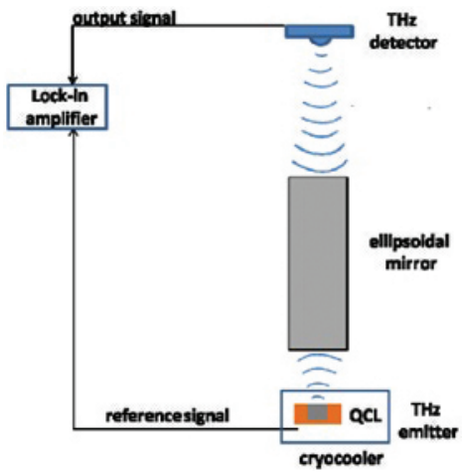

Figure 10. Sketch of a THz-CW system. A QCL is used as THz source and a bolometer or a pyrometer as THz detector.

In the following, the attention will be focused primarily on the characteristics and performance of THz measurement system working in the time domain (THz-TD). A typical architecture is shown in **Figure 11**.

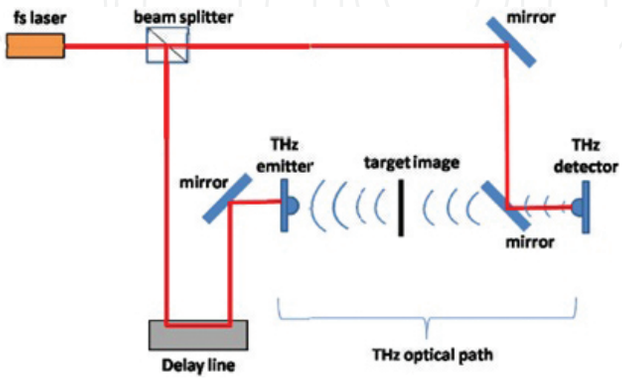

Figure 11. Typical scheme of a THz-TD system in transmission mode.

A beam splitter is adopted to divide the ultrafast optical pulse generated by an ultrafast laser into two beams, referred to as probe and pump, respectively. T-ray pulsed radiation is stimulated at the emitter by the optical pump beam via either charge transport or optical rectification effect, according to the specific type of exploited emitter. A suitable set of lenses and a pair of parabolic mirrors is adopted in this configuration to collimate and focus the diverging T-ray beam on the sample of interest. A similar combination of lenses and mirrors is then needed to recollimate and focus onto the receiver the T-ray beam passed through the sample. At receiver side, the originally split probe beam acts as an optical gate for the T-ray receiver; the optical gate signal is characterized by a shorter time duration compared with that of the arriving T-ray pulse. It is worth noting that a proper synchronization between the gating and T-ray pulse is mandatory to assure T-ray coherent detection at a time instance. By carefully controlling the optical delay line by means of the proper micromotion of a mechanical stage, it is possible to achieve a complete temporal scan of the T-ray signal [29].

Reflection measurements can be also used for practical applications, when bulky samples are considered, that are impossible to measure in a transmission mode (see **Figure 12**) [30].

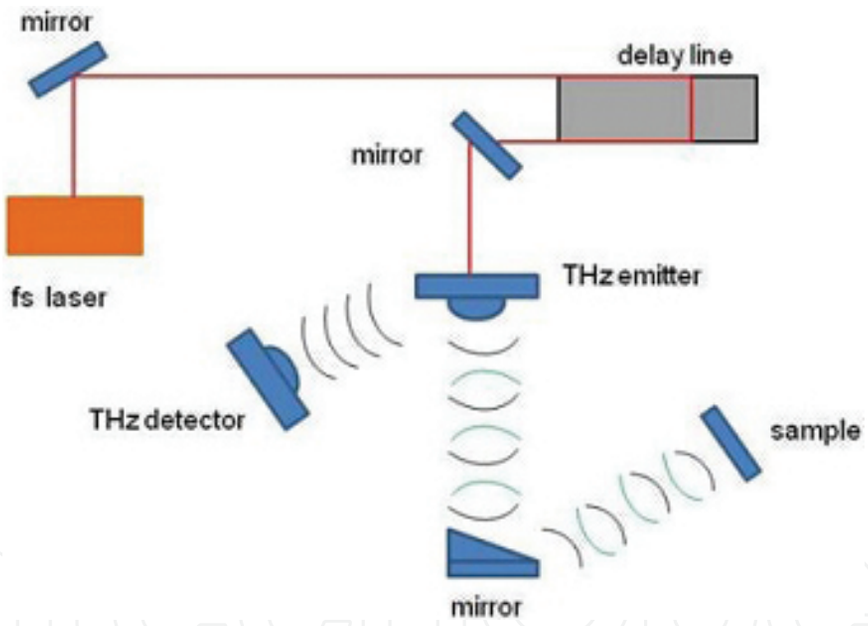

Figure 12. Typical scheme of a THz-TD system in reflection mode.

4.1. Performance of THz systems

In this paragraph, the various characteristics and limitations associated with a THz system, in particular when defining its performance, are discussed. The parameters commonly used are the dynamic range (DR) and the signal-to-noise ratio (SNR), which mainly affect the accuracy in THz measurements. They should always be evaluated during the measurements, to avoid false interpretation of the results; therefore, some recommendations for the best practice are presented [31].

http://dx.doi.org/10.5772/63734

4.1.1. Dynamic range and signal-to-noise ratio

The dynamic range (DR) is defined as the ratio between the highest and lowest measurable signal and therefore describes the maximum signal change that can be quantified. As a matter of practice, it is calculated as the ratio between the maximum signal amplitude and the root-mean-square of noise floor. The signal-to-noise ratio (SNR) is defined as the ratio between the mean peak amplitude and the standard deviation (SD) of the signal amplitude. It indicates the minimum detectable signal change and is a complementary system parameter with respect to the dynamic range. Therefore, the DR determines the measurement bandwidth, whereas the SNR reflects the amplitude resolution or sensitivity.

DR and SNR may be evaluated either with respect to the time-domain waveform or to the spectrum obtained through Fourier transform. Two specific aspects are involved when these parameters are considered. First, data are acquired as time-domain waveforms, whereas measured optical parameters are derived from the Fourier transform (FT) spectra. In particular, the DR and SNR of time-domain signals may result different from that of the corresponding spectra, and there is not a straightforward analytical relationship between the parameters estimated according to the two methods. Moreover, both DR and SNR of spectral data are strongly frequency dependent and typically decrease steeply with frequency.

The recommended procedure for estimating the DR and SNR of THz through time-domain data is based on the following steps:

1. Acquiring the time-domain waveform and measuring the maximum peak value.
2. Acquiring the noise signal in the absence of THz, for example, before the arrival of the main pulse.
3. The mean signal in the absence of THz should be constant (zero for electro-optic detection, nonzero for a photoconductive antenna). However, its standard deviation (SD) has to be measured.
4. *DR* is given by the ratio between the mean value of the measured peaks and the SD of the noisy signal.
5. *SNR* is given by the ratio between the mean value of the measured peaks and their SD.

The recommended procedure for estimating the DR and SNR of THz through the amplitude spectrum is based on the following steps:

1. Calculating the FTs of a defined number of time-domain records, their mean and SD, and estimating the noise floor of the mean FT. If only the DR is required, one FT spectrum is sufficient.
2. *DR* is given by the ratio between the mean FT amplitude and the noise floor.
3. *SNR* is given by the ratio between the mean FT amplitude and the SD.
4. The sampling frequency and observation interval of the time-domain acquisition have to be constant throughout the procedure, because both affect the SNR and the DR.

5. It is desirable to test the performance of the system by varying the scan parameters in order to identify the ranges characterized by the best SNR and DR values.

If DR and SNR are evaluated through the FT, the signal averaging is recommended, in order to reduce the noise effects. It is worth to notice that if a jitter affects the peak position, which often is due to errors in the initial position of the delay stage, the time-domain average will be distorted; the FT amplitude spectra and their average value, on the contrary, will remain correct. As expected, the approach for the evaluation of DR and SNR of a THz TDS system strictly depends on the specific domain adopted for the measurements. In other words, if the measurements are carried out in time domain, then the DR and SNR must be directly calculated from the available time-domain data. On the contrary, DR and SNR must be evaluated from FT amplitude spectra when measurement-based spectroscopic data are taken into account.

Another fundamental parameter to describe characteristics of a THz system is the spectral resolution. It is determined from the span of the time delay sweep, and it is given by the ratio between the light velocity c and the effective delay line length (multiplied by 2).

In principle, the pump laser pulse repetition rate is the only limitation of resolution if the ideal conditions of noise-free system and unlimited delay line are met. On the contrary, the actual frequency resolution is hardly reduced in presence of noise and mainly influenced by the time-domain SNR of the system. For increasing length of the delay line, the signal amplitude is reduced because of the increasing delay from the main pulse, and the SNR approaches unity.

As expected, THz pulses in the train must be identical with one another to make optical sampling works successfully. If this condition is not satisfied (i.e., the evolution of THz pulse shape occurs on time scales comparable to (or shorter than) the measurement time), no reliable samples of the waveform can be acquired. Besides this main drawback, another minor disadvantage affects the performance of optical sampling. As for the other sampling techniques, optical sampling also takes long time to acquire the desired data. The lower bound for the acquisition time is given by $N * \partial t$, (N and ∂t being, respectively, the number of measured electric fields and the train pulse-to-pulse distance). Since it is possible to take advantage of signal averaging, the acquisition time is usually much longer than this minimum value. Another problem inherent to sampling measurements is that they require a method for varying the delay of the sampling gate relative to the THz pulse. This requirement is often accomplished by means of a mechanical delay line consisting of a mirror that is moved to vary the optical path length [1].

4.1.2. TDS calibration

A typical device used for calibrating the linearity of amplitude/power measurements of THz system has to exhibit constant loss within the THz bandwidth. The most convenient and preferred solution is the employment of optically flat silicon plates as loss elements. Fresnel reflections are solely responsible for transmission losses in such a plate. Using a stack of plates parallel to each other, orthogonal to the incident THz beam and separated by air gaps, one can manage the loss level since it is dependent on the number of plates in the stack.

When the device is placed in the beam path, particular attention has to be paid to avoid distorting the THz beam or altering its focusing; in fact, it is desirable to position the device in a collimated beam. The device can be used in both THz CW and THz TDS systems, where the plates must be angled to the incident beam so as to destroy the etalon interference. There are two methods to verify the linearity and either time domain or frequency domain data can be processed:

a. In the time-domain method, the signal is processed in order to identify the peak value of the amplitude signal. Then, the obtained peaks are plotted in a semilog graph versus the number of Si plates in the beam path. The system is supposed to be linear if the plotted curve exhibits a linear behavior characterized by a slope equal to 0.7.

b. The second method of testing a TDS involves the calculation of THz spectra. The amplitude at chosen frequencies is plotted against the number of Si plates in the beam path. As in the time-domain method, the semilog plots are expected to be linear with a slope of 0.7.

It is worth noticing that the linearity of a TDS should not be assumed, but it should be experimentally verified.

4.2. Errors and uncertainty in THz-TDS

Many sources of error can affect a THz-TDS measurement and data extraction. As for example, laser intensity fluctuations, optical and electronic noise, delay line stage jitter, registration noise are common error sources. Moreover, contributions to the error in the estimated optical

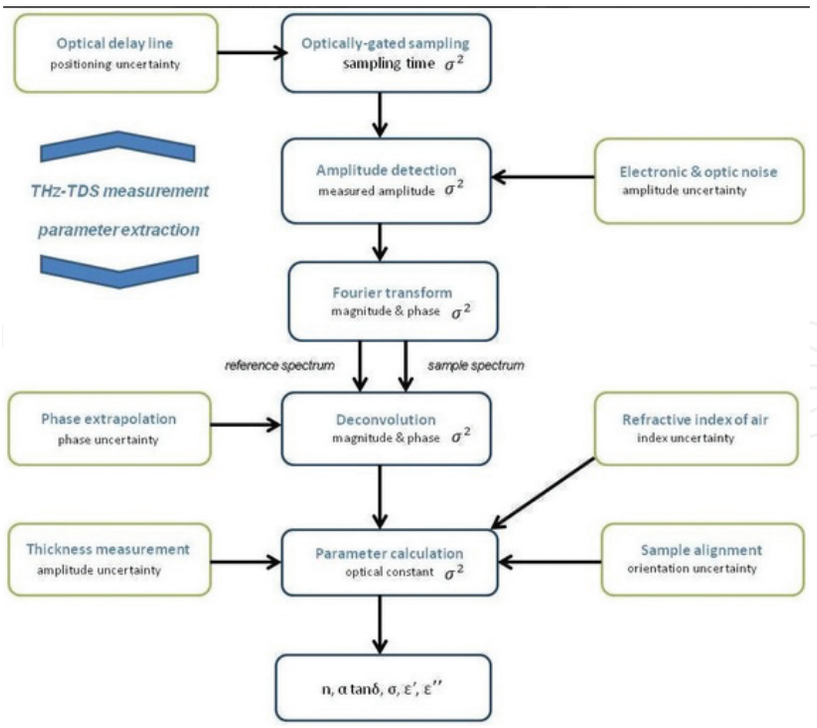

Figure 13. Scheme showing the propagation of uncertainties in THz-TDS measurements (taken from Ref. [33]).

constants are not only from the randomness in the signal, but also from imperfections in the physical setup and parameter extraction process. Examples are the sample thickness measurement, the sample alignment, and so on. Significant sources of error are shown in the scheme of **Figure 13**. The uncertainty sources (green lines) can influence both the THz-TDS measurements and the parameter extraction process. Each of them determines a variance that can be propagate along the process and determine a variance on optical constants [32, 33].

Two major sources of thermal noise can be singled out in a THz-TD system:

1. Johnson-Nyquist noise is generated when charge carriers fluctuate in a substrate. It results in an artifact voltage measured with no T-ray incident electrical field, whatever is the presence of optical gating pulses.
2. Background noise gives rise to a random voltage across the receiving antenna.

Other relevant noise sources are quantum fluctuations and laser and shot noise. One of the most efficient methods to remove noise in a T-ray signal is by means of digital signal processing technique such as wavelet de-noising that can actually improve the signal SNR, particularly when intensities are strongly reduced in biological samples. Ultimately, the noise in a THz-TDS system limits the spectral resolution; the best achievable resolution in a defined frequency interval depends, in fact, on the maximum time duration, which is, in turn, directly related to the actual SNR within that frequency range. In this way, improvement of the system dynamic range (obtained by either increasing the power of the transmitted THz waveform or decreasing the system noise floor) turns out to be mandatory to assure suitably high-frequency resolution.

Another uncertainty source is the positioning of the stage for optical delay line (ODL); thanks to the exploitation of a couple of moving mirrors, ODL mechanically induces a delay either on the probe or, equivalently, pumping pulse. As a consequence, the sampling time of the optically-gated detector is characterized by uncertainty; due to its combination with the other sources (electronic and optical noise), a final uncertainty on the amplitude measurements of the sampled T-ray pulse arises. The uncertainty associated with the amplitude of the acquired T-ray pulse affects also the spectral components obtained through the Fourier transform and the deconvolution process. Another uncertainty source that cannot be neglected involves the procedure for unwrapping the phase. Moreover, the thickness and the alignment of the samples have to be known in order to extract the model parameters; as a consequence, the uncertainty associated with these inputs affects the whole parameter detection process. Finally, the overall uncertainty is affected by the uncertainty associated with the estimation of the air refractive index. Each uncertainty source, however, can be taken into account by means of a proper model describing the uncertainty propagation in the measurement process.

4.3. THz spectroscopy

The term spectroscopy refers to a series of experiments aiming to investigate the excited states of a specimen, exploiting the interaction of a proper electromagnetic perturbation with a sample. Reflected and/or transmitted waves release specific information on the electromagnetic properties of the sample as function of the frequency. Therefore, according to the spectral content of the electromagnetic signal-probe, different excitations can be investigated ranging

http://dx.doi.org/10.5772/63734

from the quantum properties (energy levels of atomic bonds, roto-vibrational states, etc.) of molecules to the impedance of a macroscopic samples or transmission lines. The THz band is ideal to study electrodynamic properties of materials from metals to insulators, since the frequency is lower than the typical plasma frequency of metals (about 10^{15} Hz) that defines the frequency above which the metal becomes transparent to radiation. Coherent THz radiation can provide valuable information on the complete set of the complex electrodynamic parameters [34] (refractive index ($\tilde{n}$) permittivity ($\tilde{\varepsilon}$) and /or conductivity ($\tilde{\sigma}$) characterizing a material whatever it is an insulator or metallic like. The complex refractive index ($\tilde{n} = n + i\,k$) furnishes information on both the delay (n) and the absorption (k). Once n and k are obtained (see below), the permittivity $\tilde{\varepsilon} = \varepsilon_1 + i\varepsilon_2$ can be reached exploiting the following relationship $\tilde{n} = \sqrt{\tilde{\varepsilon}\,\tilde{\mu} / \varepsilon_0 \mu_0}$ where $\tilde{\mu}$ is the complex magnetic permeability, ε_0 is the vacuum permittivity, and μ_0 is the vacuum permeability. Since most of materials have $\tilde{\mu} = 1$, a direct relation between the refractive index and permittivity can be extracted $\tilde{n} \cong \sqrt{\tilde{\varepsilon}}$ which deals $n = \sqrt{\left(\sqrt{\varepsilon_1^2 + \varepsilon_2^2} + \varepsilon_1\right)/2}$ and $k = \sqrt{\left(\sqrt{\varepsilon_1^2 + \varepsilon_2^2} - \varepsilon_1\right)/2}$. Conductivity ($\tilde{\sigma} = \sigma_1 + i\sigma_2$) and permittivity are also reciprocally related through the formulas $\sigma_1 = \varepsilon_0 \omega \varepsilon_2$ and $\sigma_2 = \varepsilon_0 \omega(\varepsilon_\infty - \varepsilon_1)$, where $\omega = 2\pi\nu$ and $\varepsilon_\infty = \varepsilon\ (\omega \to \infty)$ can be obtained through a fitting procedure. From the practical point of view, the most important parameter to obtain for a sample characterization is $\tilde{n}$, since the other parameters are just a combination of n and k.

The peculiar characteristic of using a TDS consists into directly manipulating the time-dependent electric field E(x, t) transmitted through the sample. The ratio between the Fourier transforms of the transmitted signal and the reference signal is directly function of the refractive index. The sketch of the measurement on a generic sample L thick is reported in **Figure 14**. E(x,t) propagating from the transmitter (Tx) to the receiver (Rx) is linearly polarized along y. Since the signal is generated and detected in air, the proposed scheme allows to generalize the measurements in multilayer samples.

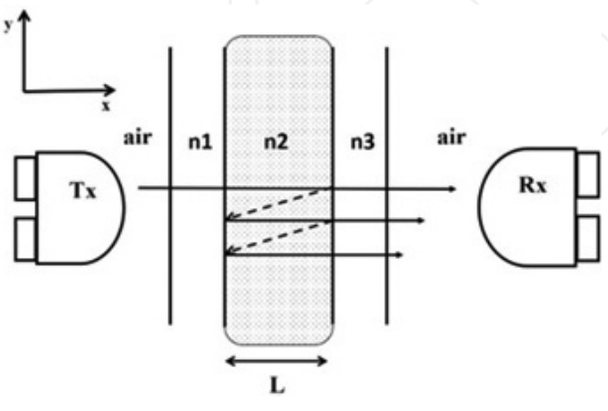

Figure 14. Scheme of the measurements through the THz-TDs system. Tx and Rx stand for transmitter and receiver, respectively. L represents the mean size of the sample, while n_i with i = 1, 2, 3 are the refractive index of different through THz pulse.

The transmitted signal through the sample $S(\omega)$, can be expressed as function of the Fresnel coefficients $T_{a,b}(\omega) = 2\tilde{n}_a/(\tilde{n}_a + \tilde{n}_b)$ and $R_{a,b}(\omega) = (\tilde{n}_a - \tilde{n}_b)/(\tilde{n}_a + \tilde{n}_b)$ and the propagation factor $P_a(\omega, d) = exp\{-i\ \tilde{n}_a\ \omega\ d\}$, where the labels refer to the material [35]. The complete signal can be expressed as:

$$S(\omega) = \eta(\omega)T_{1,2}(\omega)P_2(\omega,d)T_{2,3}(\omega)\sum_{k=0}^{\infty}\{R_{2,3}(\omega)P_2^2(\omega,L)R_{2,1}(\omega)\}^k \cdot E(\omega) \tag{5}$$

where $E(\omega)$ is the generated THz pulse, and $\eta(\omega)$ accounts for all the reflected and transmitted signals which do not reach Rx. In Eq. (1), the factors $T_{1,2}(\omega)P_2(\omega, d)T_{2,3}(\omega)$ take into account of the fraction of signal reaching Rx in one path, whereas the term $\sum_{k=0}^{K}\{R_{2,3}(\omega)P_2^2(\omega, L)R_{2,1}(\omega)\}^k$ accounts for the delayed K-pulses originated by the reflections of the primary pulse between the sample boundaries (usually $K \leq 3$). This phenomenon known as Fabry–Perot (FP) effect is depicted in **Figure 14** through the dashed arrows displaying the reflected signals. In the time domain, the FP effects show up in the appearance of copies of the primary transmitted signal. In **Figure 15**, a comparison is proposed between the reference signal (air) and the signal (Si) through a silicon slab 500 μm thick. Black arrows point out the copies of the primary signal. The delay between copies is due to the roundtrip walk in the sample and is about $\Delta t \cong 2Ln/c \sim 11.4ps$ for $n(Si) = 3.46$.

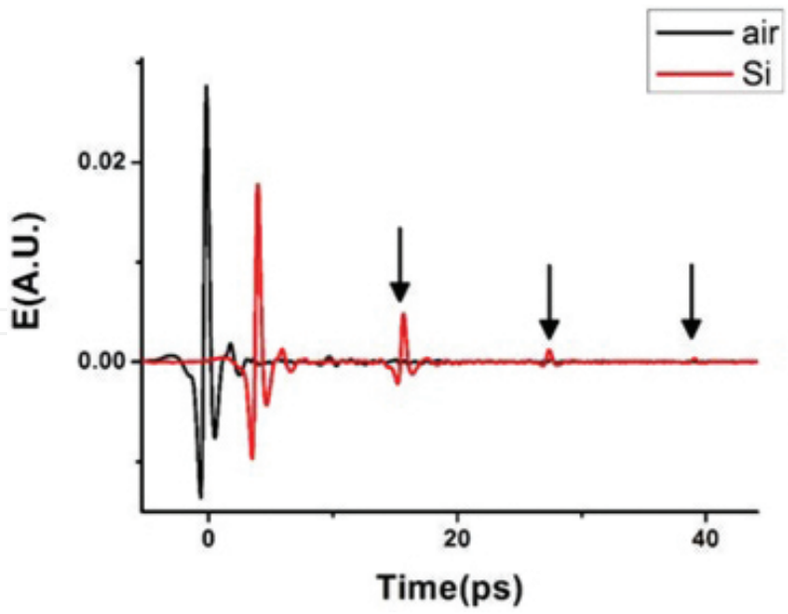

Figure 15. Time-dependent signal measured through THz-TDS system. The black curve is the reference signal acquired in free space, whereas the red curve is the signal through a Si sample of 500 μm thick. The arrows indicate the primary signal copies generated by the Fabry–Perot effect.

Eq. (1) also defines the transmittance

http://dx.doi.org/10.5772/63734

$$T(\omega) = E_{sample} \Big/ E_{ref} \tag{6}$$

that, according to Eq. (5), in the case of a simple slab can be expressed as

$$H(\omega) = \frac{2\tilde{n}_2(\tilde{n}_1 + \tilde{n}_3)}{(\tilde{n}_2 + \tilde{n}_1)(\tilde{n}_2 + \tilde{n}_3)} exp\{-\frac{i(\tilde{n}_2 - \tilde{n}_{air})\omega L}{c}\} FP(\omega) \tag{7}$$

where

$$FP(\omega) = \frac{1}{1 - (\frac{\tilde{n}_2 - \tilde{n}_1}{\tilde{n}_2 + \tilde{n}_1})(\frac{\tilde{n}_2 - \tilde{n}_3}{\tilde{n}_2 + \tilde{n}_3}) \exp\{-i\tilde{n}_2\omega 2L / c\}} \tag{8}$$

is the explicit form of the Fabry-Perot term when the echos in media 1 and 3 are negligible [35].

The transfer function $H(w)$ in Eq. (7) is used as theoretical reference for $T(\omega)$ to calculate optical parameters of samples. Eqs. (6) and (7) describe the transmission through a homogeneous slab with refractive index $\tilde{n}_2$ when the equivalence $\tilde{n}_1 = \tilde{n}_3\ \tilde{n}_{air}$ is verified. Instead by putting $\tilde{n}_1 = \tilde{n}_{air}$, Eqs. (6) and (7) are able to describe a system composed by two layers as a thin metallic film on a dielectric substrate [36, 37].

Several techniques [36–40] have been developed in order to extract $\tilde{n}$ by computing the minimum difference between the moduli and the phases of $H(\omega)$ and $T(\omega)$:

$$\delta\rho(\omega) = |H(\omega)| - |T(\omega)|$$

$$\delta\varphi(\omega) = \arg[H(\omega)] - \arg[T(\omega)] \tag{9}$$

Eq. (9) allows to define an error function, the total variation (TV) [38], defined by the sum of differences $\delta 1$ and $\delta\psi$ for each frequencial point

$$ER = \sum\nolimits_{\omega} |\delta\rho(\omega)| + |\delta\varphi(\omega)| \tag{10}$$

This is a tridimensional paraboloid as function of the frequency and the sample thickness. The computational search of the minimum of $ER(L, \omega)$ implies the contemporary knowledge of the main quantities describing the system: the sample thickness L the refractive index n, and the extinction coefficent k [39]. A fast resolution of the TV approach is affected by the noise in the measured spectrum of $T(\omega)$. The most relevant noise source in thin samples is the Fabry–Perot oscillations which show a frequency inversely proportional to L. This problem can be overcome

imposing the quasi-space (QS) optimization [39], where the periodicity of the FP effect is employed to achieve the effective optical thickness of the sample. The quasi-space is defined by the Fourier transform of an electro dynamical parameter $y(\omega_n)$ which could be the refractive index or the extinction coefficient. Therefore, a new set of variables can be defined as follows

$$Q_{S_k} = \sum_{n=1}^{N-1} [y(\omega_n) \exp(-i \frac{2\pi}{N} k\, n)], k = 0,1,2\ldots, N-1 \tag{11}$$

This function can be displayed in terms of the variable $L_{Q_S} = x_{Q_S} c_0 / 2$, where c_0 is the speed of light in vacuum and $x_{Q_S} = 2\pi/\omega$, showing a pronounced peak at the effective optical length. Alternatively, the sample thickness L can be accounted by locating the minimum of Q_{S_k} (at a fixed frequency) for different L values [40]. The QS approach is limited just by the performances of the TDS system. In particular, the maximum and minimum detectable thickness can be expressed as $L_{max} = c_0/4n\ df$ and $L_{min} = c_0/2n\ \Delta f$, where df is the minimum detectable frequency of the system while Δf is its bandwidth. The former thickness is based on the application of Nyquist theorem, whereas the latter is based on the resolution of neighbor QS's peaks [40]. For instance, assuming as parameters $df \cong 3$, and, as effective refractive index, $n \cong 2$, the maximum and minimum length are $L_{max} \cong 12.5$ mm and $L_{min} \cong 12.5$ μm, respectively. Whenever the best optical length is found, the quality of the retrieved electrodynamic parameter depends also by the choice of a good thickness of the sample. Thinner samples become transparent to THz radiation, whereas thick samples do not release much information because the transmitted signal is low. In Ref. [41], authors aim to find the best thickness in order to minimize the standard deviations (s_n^2, s_n^2) of electrodynamical parameter as (ω) and (ω) inherited by the standard deviations of signals $E_{sample}(t)$ and $E_{ref}(t)$ acquired in the time domain. The functions s_n^2, s_n^2 can be minimized with respect L leading to get the optimal thickness as function of the absorption coefficient:

$$L_{opt} = c_0 / \omega k(\omega) = \frac{2}{\alpha(\omega)} \tag{12}$$

Eq. (12) shows that $n(\omega)$ and $k(\omega)$ are affected by some indetermination as consequence of the fixed extension of the sample. On the other hand, Eq. (12) enables the possibility to get reliable results also on very thin samples provided that the absorption coefficient $\alpha(\omega)$ is enough high. Indeed, full two-dimensional systems like single graphene layers have been extensively investigated through THz-TDS systems thanks to the robust absorption coefficient $\alpha_{graphene} \sim 5$ μm^{-1} [42–44].

5. Conclusions

Without claiming to be exhaustive, we presented a short overview of THz measurement systems presently under development for scientific and industrial applications. We first described the most common sources and detectors that are routinely in use for the manipulation of T-waves. We then focused on the typical architectures that are presently employed in time-domain spectroscopy and imaging. The importance of metrological aspects in THz systems performance and measurements and most of their related issues and solutions were discussed. Since each material has its own "identity card" in this band of the spectrum, a THz-TDS waveform transmitted through a sample is typically rich in information. We therefore presented what are the main parameters that can be measured from the material frequency response, namely optical or electrical complex quantities like the refractive index, the conductivity and the dielectric constant, and what are the data extraction methods and the related errors and uncertainty.

Author details

Leopoldo Angrisani[1*], Giovanni Cavallo[2], Annalisa Liccardo[2], Gian Paolo Papari[3] and Antonello Andreone[3]

*Address all correspondence to: angrisan@unina.it

1 DIETI – Department of Information Technology and Electrical Engineering, CeSMA – Center of Advanced Measurement Services, University of Napoli Federico II, Napoli, Italy

2 DIETI – Department of Information Technology and Electrical Engineering, University of Napoli Federico II, Napoli, Italy

3 DF – Department of Physics, University of Napoli Federico II, Napoli, Italy

References

[1] Siegel P. H. THz technology: an overview. Int. J. High Speed Electron. Syst. 2003; 13(2): 351–394.

[2] Shen Y. C., Lo T., Taday P. F., Cole B. E., Tribe W. R., Kemp M. C. Detection and identification of explosives using terahertz pulsed spectroscopic imaging. Appl. Phys. Lett. 2005; 86(24): 241116.

[3] Taday P. F. Applications of terahertz spectroscopy to pharmaceutical sciences. Phil. Trans. R. Soc. Lond. A. 2004; 362: 351–364.

[4] Wilmink G. J., Grundt J. E. Terahertz radiation sources, applications, and biological effects. In: Lin J.C, editors. Handbook of Electromagnetic Fields in Biological Systems. CRC Press Taylor & Francis Group. 2012. p.369–423.

[5] Aurele J. L. A. Review of near field terahertz measurement methods and their applications. Infrared Milli Terahz Waves. 2011; 32: 976–1019.

[6] Popovic Z., Grossman E. N. THz metrology and instrumentation. IEEE Trans. Terahertz Sci. Technol. 2011; 1(1): 133–144.

[7] Kozlov G., Volkov A. Coherent Source Submillimeter Wave Spectroscopy in Millimeter and Submillimeter Wave Spectroscopy of Solid. Springer Verlag; Berlin; 1998. p. 51–109.

[8] Faist J., Sirtori C. InP and GaAs-Based Quantum Cascade in Long-Wavelength Infrared Semiconductor Lasers. John Wiley and Sons; New York; 2004. p. 217–278.

[9] Tredicucci A., Kohler R. Terahertz Quantum Cascade Lasers in Intersubband Transitions in Quantum Structures. McGraw-Hill; New York; 2006. p. 45–105.

[10] Williams B. Terahertz quantum cascade lasers. Nat. Photonics. 2007; 1: 517.

[11] Kleiner R., Steinmeyer F., Kunkel G., Müller P. Intrinsic Josephson effects in $Bi_2Sr_2CaCu_2O_8$ single crystals. Phys. Rev. Lett. 1992; 68: 2394.

[12] Ozyuzer L., Koshelev A. E., Kurter C., Gopalsami N., Tachiki Q., Li, M., Kadowaki K. Emission of coherent THz radiation from superconductors. Science. 2007; 318: 1291.

[13] Tani M., Matsuura S., Sakai K., Nakashima S. Emission characteristics of photoconductive antennas based on low-temperature grown GaAs and semi-insulating GaAs. Appl. Opt. 1997; 36(30): 7853–7859.

[14] Shen Y. C., Upadhya P. C., Beere H. E., Linfield E. H., Davies A. G., Gregory I. S. Generation and detection of ultra-broadband terahertz radiation using photoconductive emitters and receivers. Appl. Phys. Lett. 2004; 85(2): 164–166.

[15] Shen Y. C., Upadhya P. C., Linfield E. H., Beere H. E., Davies A. G. Ultra-broadband terahertz radiation from low-temperature-grown GaAs photoconductive emitters. Appl. Phys. Lett. 2003; 83(15): 3117–3119.

[16] Leitenstorfer A., Hunsche S., Shah J., Nuss M. C., Knox W. H. Detectors and sources for ultra broadband electro-optic sampling: experiment and theory. Appl. Phys. Lett. 1999; 74(11): 1516–1518.

[17] Sinyukov A. M., Leahy M. R., Hayden M., Haller M., Luo J., Jen A. K-Y. Resonance enhanced THz generation in electro-optic polymers near the absorption maximum. Appl. Phys. Lett. 2004; 85(24): 5827–5829.

[18] Sinyukov A. M., Hayden L. M. Generation and detection of terahertz radiation with multilayered electro-optic polymer films. Opt. Lett. 2002; 27(1): 55–57.

[19] Wu Q., Zhang X. C. Ultrafast electro-optic field sensor. Appl. Phys. Lett. 1996; 68(12): 1604–1606.

[20] Sands D. Diode Lasers. Taylor & Francis; London; 2004.

[21] Auston D. H., Cheung K. P., Smith P. R. Picosecond photoconducting Hertzian dipoles. Appl. Phys. Lett. 1984; 45: 284–286.

[22] Golay M. J. E. A pneumatic infrared detector. Rev. Sci. Instr. 1947; 18: 347.

[23] Cooper J. A fast-response pyroelectric thermal detector. Rev. Sci. Instr. 1962; 39: 462.

[24] Kinch M. A. Compensated silicon-impurity conduction bolometer. J. Appl. Phys. 1971; 42: 5861.

[25] Andrews D. H., Milton R. M., DeSorbo W. J.A Fast Superconducting Bolometer Opt. Soc. Am. 1946; 36(9): 518.

[26] Liu T. A., Tani M., Nakajima M., Hangyo M., Pan C. L. Ultra-broadband terahertz field detection by photoconductive antennas based on multi-energy arsenic ion implanted GaAs and semi-insulating GaAs. Appl. Phys. Lett. 2003; 83(7): 1322.

[27] Kono S., Tani M., Sakai K. Ultra-broadband photoconductive detection: comparison with free-space electro-optical sampling. Appl. Phys. Lett. 2001; 79(7): 898–900.

[28] Angrisani L., Bonavolontà F., Schiano Lo Morello R., Andreone A., Casini R., Papari G.P. First steps towards an innovative compressive sampling based-THz imaging system for early crack detection on aerospace plates. In: IEEE International Workshop on Metrology for AeroSpace (IEEE 2014); 29–30 May 2014.

[29] Withayachumnankul W., Lin H., Mickan S. P., Fischer B. M., Abbott D. Analysis of measurement uncertainty in THz-TDS. Phot. Mater. Dev. Appl. II. 2007; 6593:659326-1-18.

[30] Zhang C., Zhong H., Zhang L. A phase extraction technique for terahertz reflection spectroscopy. Proc. SPIE. 2009; 7158: 71580Q–71580Q–14.

[31] Naftaly M., Dudley R. Methodologies for determining the dynamic ranges and signal-to-noise ratios ofTerahertz time domain spectroscopy. Opt. Lett. 2009; 34(8): 1213–1215.

[32] Naftaly M. Metrology issues and solutions in THz time domain spectroscopy: noise, errors, calibration. IEEE Sens. J. 2013; 13(1): 8–17.

[33] Withayachumnankul W., Naftaly M. Fundamentals of measurement in terahertz. J. Infrared Milli. Terahz Waves. 2014; 35: 610–637.

[34] Hangyo M. Development and future prospects of terahertz technology. Jpn J. Appl. Phys. 2015; 54: 120101.

[35] Duvillaret L., Garet F., Coutaz J. L. A reliable method for extraction of material parameters in terahertz time-domain spectroscopy. IEEE J. Selected Top. Quantum Electron. 1996; 2(3): 739-746.

[36] Yasuda H., Hosako I. Measurement of terahertz refractive index of metal with terahertz time-domain spectroscopy. Jpn J. Appl. Phys. 2008; 47: 1632–1634.

[37] Zhou D. X., Parrott E. P. J., Douglas J. P., Zeitler J. A. Determination of complex refractive index of thin metal films from terahertz time-domain spectroscopy. J. Appl. Phys. 2008; 104: 053110.

[38] Dorney T. D., Baraniuk R. G., Mittleman D. M. Material parameter estimation with terahertz time-domain spectroscopy. J. Opt. Soc. Am. A. 2001; 18(7): 1562-1571.

[39] Pupeza I., Wilk R., Koch M. Highly accurate optical material parameter determination with THz time-domain spectroscopy. Optics Express 2007; 15: 4335.

[40] Scheller M., Jansen C., Koch M. Analyzing sub-100-lm samples with transmission terahertz time domain spectroscopy. Opt. Commun. 2009; 282: 1304–1306.

[41] Withayachumnankul W., Fischer B. M., Abbott D. Material thickness optimization for transmission-mode terahertz time-domain spectroscopy. Opt. Express 2008; 16(10): 7382.

[42] Kuzel P., Nemec H. Terahertz conductivity in nanoscaled systems: effective medium theory aspects. J. Phys. D: Appl. Phys. 2014; 47: 374005.

[43] Ivanov I., Bonn M., Mics Z., Turchinovich D. Perspective on terahertz spectroscopy of graphene. Eur. Phys. Lett. 2015; 111: 67001.

[44] Denisultanov A. K., Azbite S. E., Balbekin N. S., Gusev S. I., Khodzitsky M. K. Optical properties of graphene on quartz and polyethylene substrates in terahertz frequency range. PIERS Proceedings, Guangzhou, China, August 25–28, 2014.